Atmospheric Research 255 (2021) 105533

Contents lists available at ScienceDirect

Atmospheric Research

journal homepage: www.elsevier.com/locate/atmosres

Historical fidelity and future change of Amundsen Sea Low under 1.5 °C–4 °C global warming in CMIP6

Miaoni Gao [a,*], Seong-Joong Kim [b], Jing Yang [c], Jiping Liu [d], Tong Jiang [a], Buda Su [a], Yanjun Wang [a], Jinlong Huang [a]

[a] Institute for Disaster Risk Management, School of Geographical Sciences, Nanjing University of Information Science and Technology, Nanjing, China
[b] Division of Polar Climate Sciences, Korea Polar Research Institute, Incheon, South Korea
[c] Faculty of Geographical Science, Beijing Normal University, Beijing 100875, China
[d] Department of Atmospheric and Environmental Sciences, University at Albany, State University of New York, USA

ARTICLE INFO

Keywords:
Amundsen Sea Low
CMIP6
Historical Fidelity
Future Projection
Global Warming Levels

ABSTRACT

The realistic simulation and projection of the Amundsen Sea Low (ASL) are essential for understanding the Antarctic climate and global climate change. Using 14 models that participated in phase 6 of the Coupled Model Intercomparison Project (CMIP6), this study evaluates the climatological characteristics of ASL with comparison to the ERA5 reanalysis and their CMIP5 versions and assesses the future change of ASL under 1.5 °C–4 °C global warming. The climatological spatial distribution of ASL is captured reasonably but with underestimated intensity by CMIP6 multi-model ensemble (MME). Among the CMIP6 models, EC-Earth3 has most accurate representation of ASL according to the pattern correlation and biases. The seasonal variation of the ASL depth and location are found to be reasonably reproduced by the CMIP6 models. CMIP6 MME has higher skills in simulating the seasonal cycle of absolute depth and zonal migration of the ASL center. The relative central pressure of ASL is underestimated in all seasons and there is a 4-degree northward shift bias of the ASL center in austral winter, which were also evident in the CMIP5. The semiannual cycle of ASL absolute depth with two deepest pressure in April and October is also captured by CMIP6 MME. However, the observed peak of pressure between the two months occurs in June, while it delays one month and appears until July in CMIP6 MME. Compared with CMIP5, CMIP6 MME exhibit evident reduced uncertainties and overall improvement in simulating absolute depth and location of the ASL center, which might be attributed to models' capability of representing the location of Southern Hemisphere westerlies, while the biases in relative depth become even large in CMIP6 MME. In response to future warming from 1.5 °C to 4 °C above pre-industrial levels, the absolute depth of ASL will very likely deepen with larger amplitude in all seasons, while the relative depth might enhance only under high-level warmer world in austral autumn to winter. The CMIP6 MME also projects that the ASL will shift poleward constantly in austral summer and migrate southwestward during austral autumn with the rising global mean temperature. Among all the seasons, the most prominent future changes in intensity and location of ASL are found in autumn. The enhancement and poleward movement of ASL could also be identified during the Ross Sea ice advance season under 1.5 °C–4 °C global warming. The results reveal the potential of CMIP6 models in the ASL study and the impact of ASL on Antarctic climate under different global warming levels.

1. Introduction

Amundsen Sea Low (ASL) is a climatological low pressure system located in the latitude band 60–70°S over Pacific sector of the Southern Ocean, which comprises the Ross Sea, Amundsen Sea and Bellingshausen Sea (Raphael et al., 2016). Different from Southern Annular Mode (SAM), which is the dominant mode around Antarctica describing the north-south pressure gradient, ASL is a nonzonal circulation induced by the interaction of the mean westerly flow with the high orography of Victoria Land. It has profound impacts on climate of West Antarctica through modifying meridional winds, including sea ice concentration, temperature, and precipitation (e.g., Hosking et al., 2013; Raphael and

* Corresponding author at: Institute for Disaster Risk Management, School of Geographic Sciences, Nanjing University of Information Science and Technology, Nanjing 210044, China.
E-mail address: gaomn@nuist.edu.cn (M. Gao).

https://doi.org/10.1016/j.atmosres.2021.105533
Received 15 December 2020; Received in revised form 5 February 2021; Accepted 17 February 2021
Available online 24 February 2021

Landrum, 2019; Wang et al., 2020a, 2020b). Since the Antarctic climate plays an important role in Earth's system (e.g., Bronselaer et al., 2018; Roussel et al., 2020), the realistic simulation, prediction and projection of ASL is critical for understanding and projecting Antarctica climate change.

Coupled global climate model is one of the primary tools used in studies of climate dynamics and change, as well as the Antarctic climate (e.g., Gao et al., 2016; Jun et al., 2020; Luo et al., 2020; Shu et al., 2020). Numerous models were convened to better understand and project the climate under the coordination of Climate Model Intercomparison Project (CMIP). Hosking et al. (2013) evaluated the ASL characteristics simulated by 17 CMIP5 models with a focus on the annual cycle of relative depth and longitude of the ASL center and reported that majority of them have substantial biases. Currently, the Intergovernmental Panel on Climate Change (IPCC) is working on the Sixth Assessment Report which will be drafted referring to results of the sixth phase of CMIP (CMIP6). After nearly a decade of model development relative to CMIP5, three aspects of improvement were noticed in CMIP6, including: (1) there are new modelling centres registered to provide simulations, (2) coupled global climate models were designed with finer resolution and improved physical processes, and (3) the Shared Socio-economic Pathways (SSP) combined with the Representative Concentration Pathways of CMIP5 are used as the new future scenarios for climate change projection (The CMIP6 landscape, 2019). The newly released output of CMIP6 experiments offer us a great opportunity to examine whether the CMIP6 models have a better performance in simulating ASL.

Antarctic climate has gained a widely attention because of the high albedo of the ice and large potential source for global sea-level rise (e.g., Garbe et al., 2020; Jun et al., 2020). Recent studies found that the ASL is deepening during 1979–2006, which plays an important role in the increasing trend of sea ice concentration over the Ross Sea (Turner et al., 2009). Furthermore, the models' capability of representing west Antarctic climate was reported to be determined by their skills in simulating ASL (Hosking et al., 2013). The close linkage between ASL and Antarctic climate makes assessing the future change of ASL crucial for understanding Antarctic climate variability, especially sea ice.

The United Nations Framework Convention on Climate Change proposed to limit the increase in the global mean temperature rise in order to reduce the impacts and risks brought by climate change in the Paris Agreement in 2015, which are devoted to hold the increase in global temperature to below 2 °C above pre-industrial levels and pursue efforts to limit the global-mean temperature increase to below 1.5 °C by the end of 21st century (United Nations Framework Convention on Climate Change, 2015). From that time forward, the possible future climate change and its impacts under 1.5 °C and 2 °C warming thresholds were widely explored and summarized by IPCC Special Report on the impacts of global warming of 1.5 °C above pre-industrial levels (IPCC, 2018; King and Harrington, 2018; Su et al., 2018). However, Raftery et al. (2017) have pointed out the range of global temperature increase might be 2.0–4.9 °C in 2100 and there is only a 5% chance that it will be controlled below 2 °C. To make better preparation for climate change adaption, climate tipping points have drawn extensive attention, by which increasing numbers of studies focus on climate change under more serious warming levels including 3 °C and 4 °C (Dosio and Fischer, 2018; Lenton et al., 2019). Based on Representative Concentration Pathway experiments in CMIP5, Raphael et al. (2016) have found that the relative depth of ASL will likely become deeper in all seasons except for summer with increasing radiative forcing. Meanwhile, ASL will likely migrate poleward in austral summer and autumn, and eastward in autumn and winter during the second half of the 21st century (Hosking et al., 2016). However, the possible changes of ASL under different global warming thresholds would allow us to identify the climate tipping points and define the climate emergency and strengthens that we remain unclear.

The aims of this study are to (1) evaluate the models' capabilities in

Table 1
A brief description of CMIP5 and CMIP6 models used in this study.

Institute, Country	CMIP5		CMIP6	
	Models	Horizontal Resolution (lat*lon)	Models	Horizontal Resolution (lat*lon)
Commonwealth Scientific and Industrial Research Organization/ Bureau of Meteorology, Australia	ACCESS1.0	145 × 192	ACCESS-ESM1–5	145 × 192
Beijing Climate Centre, China Meteorological Administration, China	BCC-CSM1–1	64 × 128	BCC-CSM2-MR	160 × 320
Canadian Centre for Climate Modelling and Analysis, Canada	CanESM2	64 × 128	CanESM5	64 × 128
National Centre for Atmospheric Research, USA	CESM1-WACCM	96 × 144	CESM2-WACCM	192 × 288
Irish Centre for High-End Computing, Netherlands/Ireland	EC-Earth	160 × 320	EC-Earth3	256 × 512
National Oceanic and Atmospheric Administration, Geophysical Fluid Dynamics Laboratory, USA	GFDL-ESM2M	90 × 144	GFDL-ESM4	180 × 288
National Aeronautics and Space Administration-Goddard Institute for Space Studies, USA	GISS-E2-R	90 × 144	GISS-E2–1-G	90 × 144
Russian Academy of Sciences, Institute of Numerical Mathematics, Russia	INMCM4.0	120 × 180	INM-CM5–0	120 × 180
Institut Pierre Simon Laplace, France	IPSL-CM5A-LR	96 × 96	IPSL-CM6A-LR	143 × 144
Atmosphere and Ocean Research Institute (The University of Tokyo), National Institute for Environmental Studies and Japan Agency for Marine-Earth Science and Technology, Japan	MIROC5	128 × 256	MIROC6	128 × 256
Max Planck Institute for Meteorology, Germany	MPI-ESM-MR	96 × 192	MPI-ESM1–2-HR	192 × 384
Meteorological Research Institute, Japan	MRI-ESM1	160 × 320	MRI-ESM2–0	160 × 320
Bjerknes Centre for Climate Research, Norwegian Meteorological Institute, Norway	NorESM1-M	96 × 144	NorESM2-LM	96 × 144
Institute of Atmospheric Physics, Chinese Academy of Sciences, China	/	/	FGOALS-f3-L	180 × 288

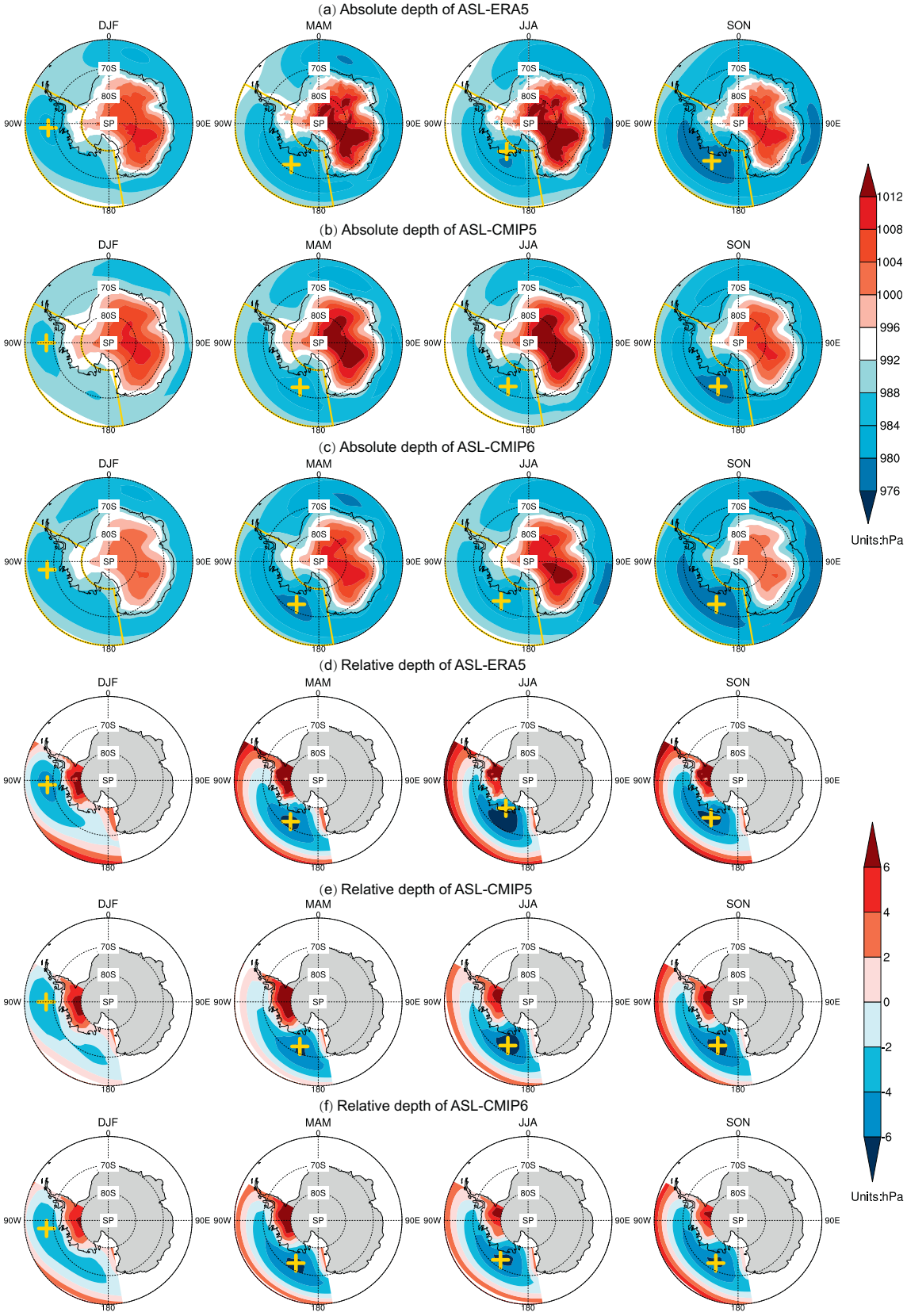

Fig. 1. (a-c) Actual mean sea level pressure and (d-f) relative mean sea level pressure (hPa) averaged in DJF, MAM, JJA, and SON during 1979–2005 in (a)/(d) ERA5 reanalysis, (b)/(e) CMIP5 MME and (c)/(f) CMIP6 MME, respectively. The yellow rectangles in (a)-(c) and the yellow crosses denote the ASL regions and centers, respectively.

simulation climatological features of ASL and examine whether the current-day climate models improve their skills, and (2) assess how the ASL will change under 1.5 °C–4 °C global warming above pre-industrial levels using 14 newly released CMIP6 models. The remainder of this paper is organized as follows. A detailed description of the models, data and methods used is given in section 2. The evaluation of historical simulations in climatological characteristics of ASL against the observation and the comparison between the performance in CMIP6 and CMIP5 models are presented in section 3. Section 4 assesses future changes of ASL under 1.5 °C–4 °C warming scenarios. Discussion and conclusion are presented in sections 5.

2. Data and methodology

2.1. Data

Due to the lack of long-term in-situ observations over the Amundsen, Bellingshausen and Ross Seas, the monthly mean sea level pressure with a horizontal resolution of 0. 25° spanning 1979–2014 from the latest version of reanalysis dataset produced by the European Centre for Medium-Range Weather Forecasts (ERA5), was used to identify the observed ASL features (Hersbach et al., 2020).

The performance of newly released global climate models in the ASL simulation participating in CMIP6 were evaluated against ERA5 and compared to their CMIP5 versions to lay a baseline for assessing future changes (Eyring et al., 2016; see Table 1 for detailed information). Only the first ensemble member (r1i1f1p1) from one model with available monthly mean sea level pressure from each institute was selected and total 14 models were used in this study. The monthly mean sea level pressure during 1979–2014 and 1979–2005 were obtained from the historical run of the CMIP6 and CMIP5 models, respectively. The future projections were performed by using monthly mean sea level pressure for 2015–2100 under SSP1–1.9, SSP1–2.6, SSP2–4.5, SSP3–7.0, SSP4–6.0, SSP5–8.5 scenarios from abovementioned models and FGOALS-f3-L provided by the Scenario Model Intercomparison Project (ScenarioMIP) belonging to CMIP6 (O'Neill et al., 2016) (Table S1). The monthly mean surface air temperature during 1850–2014 from historical run and 2015–2100 under SSPs scenarios were also used to identified the timings of the 1.5 °C-4°Cwarming levels. All the analysis in this study were based on the first ensemble member of all experiments derived from both CMIP5 and CMIP6.

2.2. Methodology

2.2.1. ASL indices

According to Hosking et al. (2013), four indices were used to describe ASL features, including Actual Central Pressure (ACP), Relative Central Pressure (RCP), longitude (LON) and latitude (LAT). The ACP and RCP are the pressure of the ASL center, which refer to the minimum values of actual and relative pressure over the region spanning 62°W–170°E (170–298°E), 80–60°S, respectively (Hosking et al., 2016). Since ASL is influenced by but separable from large-scale variability, the RCP was intentionally defined to remove signals such as the SAM across the ASL sector region. Thus, the relative pressure was calculated by subtracting representative background pressure averaged over the abovementioned domain from actual mean sea level pressure. The location of ASL was quantified by the longitude and latitude of ASL center.

This study mainly focuses on the ASL characteristics in four seasons. Austral summer, autumn, winter, and spring refer to December-January-February (DJF), March-April-May (MAM), June-July-August (JJA), and September-October-November (SON), respectively. Since sea ice plays an important role in the Earth's climate system and is significantly related with ASL over the Ross Sea in the sea ice advance season, the evolution of ASL during the Ross sea ice advance period defined as March to August were further analyzed purposely (Raphael and Landrum, 2019).

2.2.2. Definitions of 1.5 °C, 2 °C, 3 °C and 4 °C warmer worlds

For each of the model runs under each scenario, the periods of 1.5 °C, 2 °C, 3 °C and 4 °C warming levels above the preindustrial levels (1850–1900) were identified using 20-year running average global mean surface air temperature from spliced historical run-SSPs simulations before 2100 (IPCC, 2018; Zhang et al., 2018). As a result, 68, 59, 36 and 16 20-year running averages were selected as 1.5 °C, 2 °C, 3 °C and 4 °C warming levels periods, respectively (Table S2).

2.2.3. Data processing and statistical analysis

All calculations based on the CMIP model outputs were conducted on native grids in the models except when spatial patterns are shown (Zhang et al., 2018). The spatial distribution of ASL was obtained after the data were interpolated into a uniform resolution 2.5° × 2.5°. The multi-model ensemble (MME) was calculated by averaging the results of each model using equivalent weights.

To have a straight comparison of the ASL simulated by CMIP6 models and their CMIP5 versions, the Taylor diagram showing pattern correlations (R) and the ratios of the normalized standard deviation of CMIP models against observation (SDR) was applied (Taylor, 2001). The skill score proposed by Chen et al. (2013) given by the following formula was further used to obtain a simple and intuitionistic expression of CMIP6 models' abilities in reproducing ASL with taking both spatial distribution and magnitude into consideration:

$$Skill\ Score = \frac{(1+R)^2}{\left(SDR + \frac{1}{SDR}\right)^2}.$$

Thus, the perfect model's skill score is 1. The closer the skill score is to 1, the better the model's performance. Then we ranked all the CMIP6 models on the basis of their skill scores of ASL in all seasons from 1 to 14 and calculate a comprehensive rating index (CRI) following Jiang et al. (2015),

$$\mathrm{CRI} = 1 - \frac{1}{nm}\sum_{i=1}^{n} rank_i,$$

where m is the number of models, n the number of seasons. Correspondingly, the closer to 1 the value of CRI, the higher the skill of the simulation.

Following the latest IPCC report which used 1986–2005 as baseline (IPCC, 2018), the baseline is updated from 1995 to 2014 in this study. To remove the system bias of the CMIP6 models, the changes of ASL in the future were calculated by subtracting ASL indices simulated in the baseline from the projections under different warming levels based on CMIP6 output. The changes were considered significant when the changes of MME are significant at 95% confidence level based on Student's *t*-test and more than 70% of the model runs agree on the sign of MME (Dosio and Fischer, 2018; Wang et al., 2020).

3. Historical fidelity of ASL simulated by CMIP6 models and their CMIP5 versions

The performance of ASL was comprehensively evaluated in the 13 CMIP6 models and their CMIP5 versions and FGOALS-f3-L model against observation, with a focus on the depth and location of ASL.

3.1. Spatial distribution

Fig. 1a-c shows the spatial distribution of observed and simulated ASL based on actual sea level pressure averaged in DJF, MAM, JJA and SON during 1979–2005. The observed absolute mean sea level pressure in the high latitude shows a strong north-south pressure gradient. ASL is the deepest of three pressure centers around Antarctica, especially in

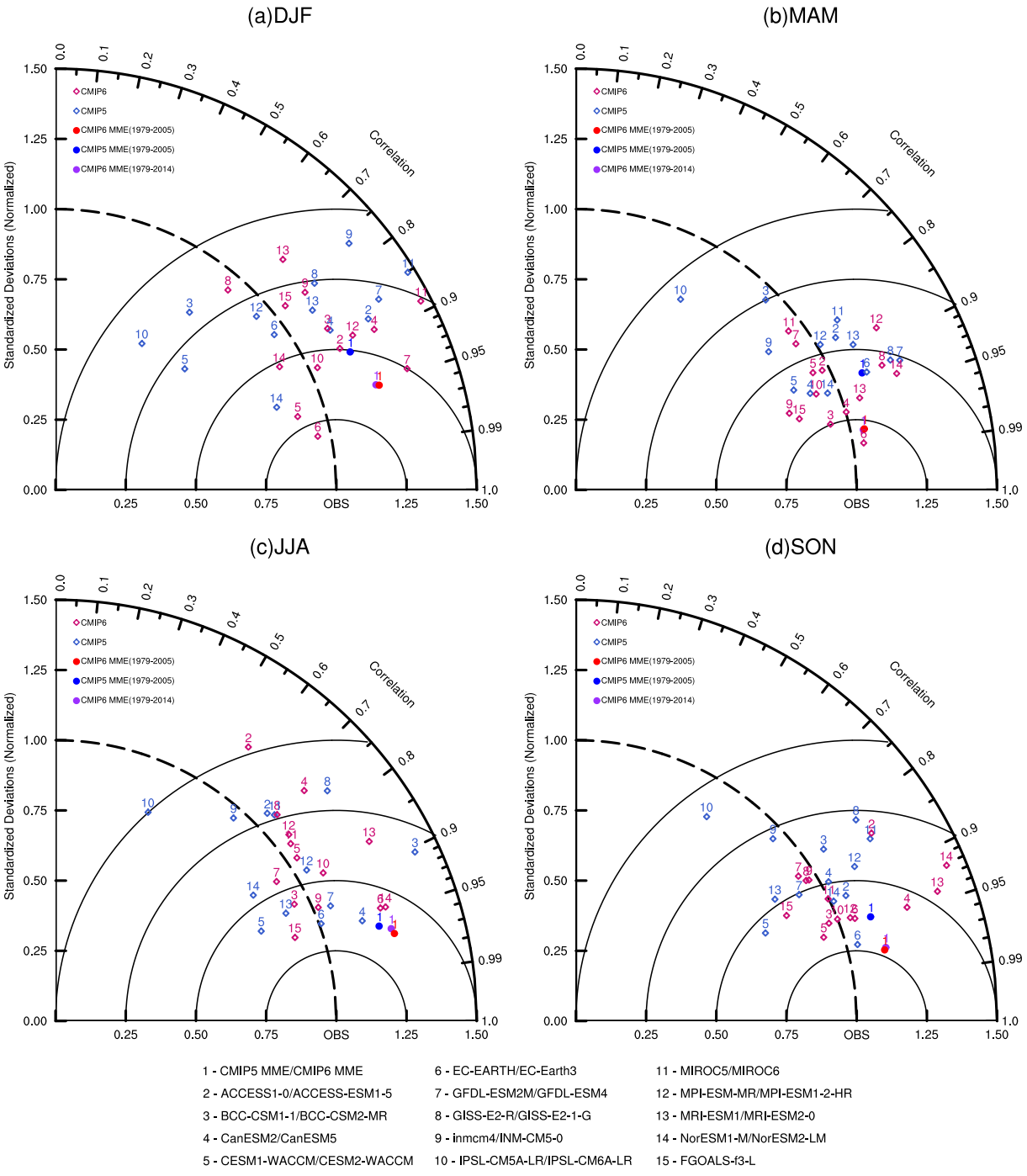

Fig. 2. Tylor diagram of ASL in CMIP5/CMIP6 models against the ERA5 dataset. Red rhombbuses and dots denote results of individual CMIP5 models and CMIP5 MME during 1979–2005, respectively. Blue rhombbuses and dots denote results of individual CMIP6 models and CMIP6 MME during 1979–2005, respectively. The purple dot represents CMIP6 MME during 1979–2014.

austral spring. Overall, both of CMIP5 and CMIP6 MME could reproduce this feature reasonably. The depth of ASL simulated by CMIP5 MME is underestimated in all seasons, but it has been improved by CMIP6 MME. The obvious westward shift of the ASL center from the Bellingshausen Sea in austral summer across the Amundsen Sea to the Ross Sea in winter is also captured by CMIP models. To separate the signal of ASL from atmospheric large-scale variability in the background, the relative sea level pressure was also investigated (Fig. 1d-f). In contrast to actual pressure, the relative pressure in the ASL sector region is generally captured but underestimated around the ASL center by both of CMIP5 and CMIP6 MME.

The Taylor diagram was further applied to examine the CMIP models' skills in simulating the spatial distribution of ASL in terms of pattern correlations and the ratios of the normalized standard deviation between models and observation. There are two prominent features identified from Fig. 2. One is that dots representing CMIP6 models locate closer to the ERA5 than CMIP5, indicating higher pattern correlations and less biases. The other is that CMIP MMEs show higher skills in reproducing the spatial distribution of ASL than individual models. The pattern correlation coefficients of relative pressure in ASL sector between each CMIP5 models and ERA5 vary between 0.51 and 0.94, 0.48–0.93, 0.41–0.95 and 0.54–0.97 in DJF, MAM, JJA and SON, while

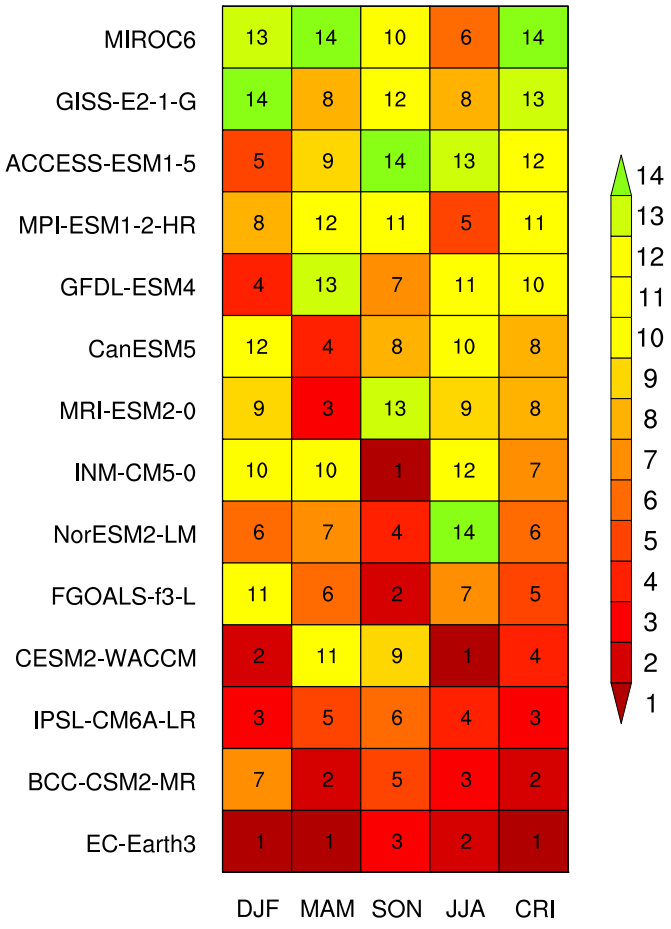

Fig. 3. Ranks of skill scores of ASL spatial distribution in four seasons and CRI during 1979–2014 derived from individual CMIP6 models.

the coefficients between their CMIP6 versions and observation are 0.65–0.98, 0.8–0.99, 0.58–0.95 and 0.84–0.95, respectively. The correlation coefficients between CMIP MME and observation increase from 0.91, 0.93, 0.96 and 0.94 in CMIP5 to 0.95, 0.98, 0.97 and 0.97 in CMIP6 during four seasons. In contrast, the biases defined as the distance of SDR from 1 derived from CMIP5 models spread from 0.04–0.47, 0.01–0.24, 0.01–0.41, 0.01–0.26, and turns into 0.03–0.46, 0–0.22, 0.02–0.29,0–0.43 in CMIP6. That means that biases increase from 0.15, 0.2 and 0.11 in CMIP5 MME to 0.21, 0.25 and 0.13 in CMIP6 MME during DJF, JJA and SON, except for that in MAM decrease from 0.1 to 0.05. Although the ratios of variance become larger in austral spring, summer, and winter, the statistical bias based on Taylor diagram according to the combined results of pattern correlation and variance of CMIP6 MME during 1979–2005 is smaller than that in CMIP5. Briefly, the spatial distribution of ASL simulated by CMIP6 models are in better agreement with observation than CMIP5 models. Among all the seasons, CMIP6 models make largest improvement in reproducing ASL in MAM, which results in the best ability of CMIP6 MME in austral autumn. In addition, we also intentionally checked the simulation of relative pressure in ASL sector during the recent decade based on the CMIP6 MME from 1979 to 2014, which indicates different target periods of evaluation barely influences the result.

We further ranked the CMIP6 models according to the skill scores by taking their performances in all seasons during 1979–2014 into account to quantify their capabilities in capturing spatial distribution of ASL (Fig. 3). Thus, the CMIP6 models were sorted by their performance of reproducing ASL, which are EC-Earth3, BCC-CSM2-MR, IPSL-CM6A-LR, CESM2-WACCM, FGOALS-f3-L, NorESM2-LM, INM-CM5–0, MRI-ESM2–0, CanESM5, GFDL-ESM4, MPI-ESM1–2-HR, ACCESS-ESM1–5, GISS-E2–1-G and MIROC6 from best to relatively poor skills based on their first ensemble member, respectively.

3.2. Annual cycle of ASL depth and location

A well-defined annual cycle of ASL could be found in Fig. 1. Hence, four indices, including ACP, RCP, LAT and LON, were used to quantify the seasonal evolutions of ASL (Fig. 4). Distinct features of ASL intensity are identified based on two types of indices, which are the absolute and relative pressure of the ASL center, respectively. Compared to ACP, RCP is separable from large-scale variability such as SAM and El Niño-Southern Oscillation (ENSO) since the representative background pressure averaged over the ASL sector region has been subtracted (Hosking et al., 2016). In observation, the absolute depth of ASL is 983.2 hPa in austral summer, then deepens gradually with seasons and reaches its lowest pressure of 976.3 hPa in the following spring (Fig. 4a). By contrast, the relative depth of ASL shows a maximum and minimum in austral summer and winter, which is −4.8 hPa and − 7.8 hPa, respectively (Fig. 4b). In general, the seasonal evolution of ASL depth is well represented by CMIP5 and CMIP6 MME. But the simulation skills of CMIP models in capturing ACP is higher than that of RCP, because the RCP is underestimated by CMIP5 and CMIP6 models in all seasons, especially the pressure in austral winter.

The latitude and longitude of ASL center were also analyzed based on LAT and LON because previous studies pointed out that the location of ASL has a tremendous impact on Antarctic climate (Hosking et al., 2013). According to ERA5, the ASL center locates at its northernmost point of 68°S in austral summer, moves southward gradually and

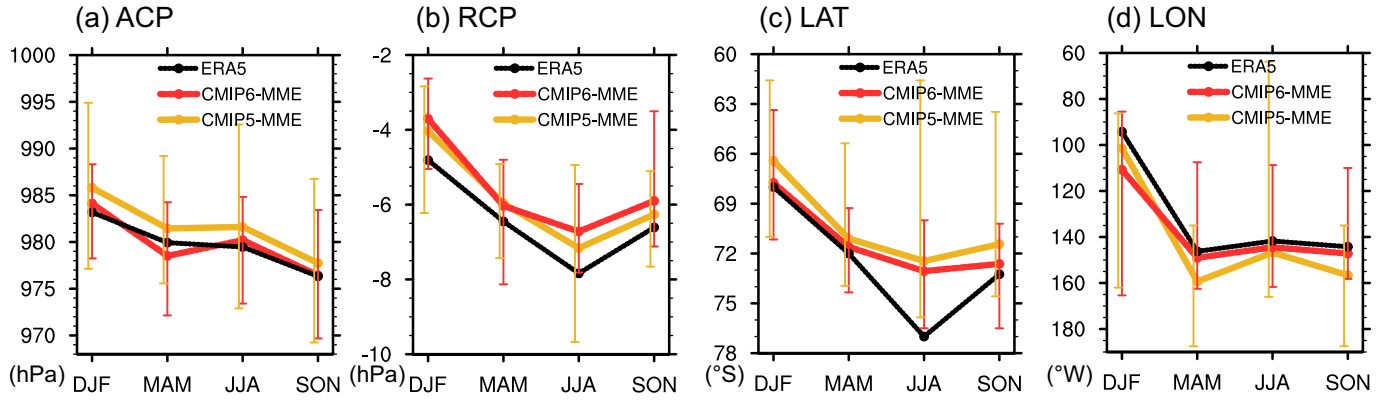

Fig. 4. Seasonal evolution of the (a) ACP, (b) RCP, (c) LAT, and (d) LON of ASL observed in ERA5 reanalysis (black), CMIP5 MME (red) and CMIP6 MME (yellow) during 1979–2005, respectively. The vertical lines show the band of ASL indices in individual models.

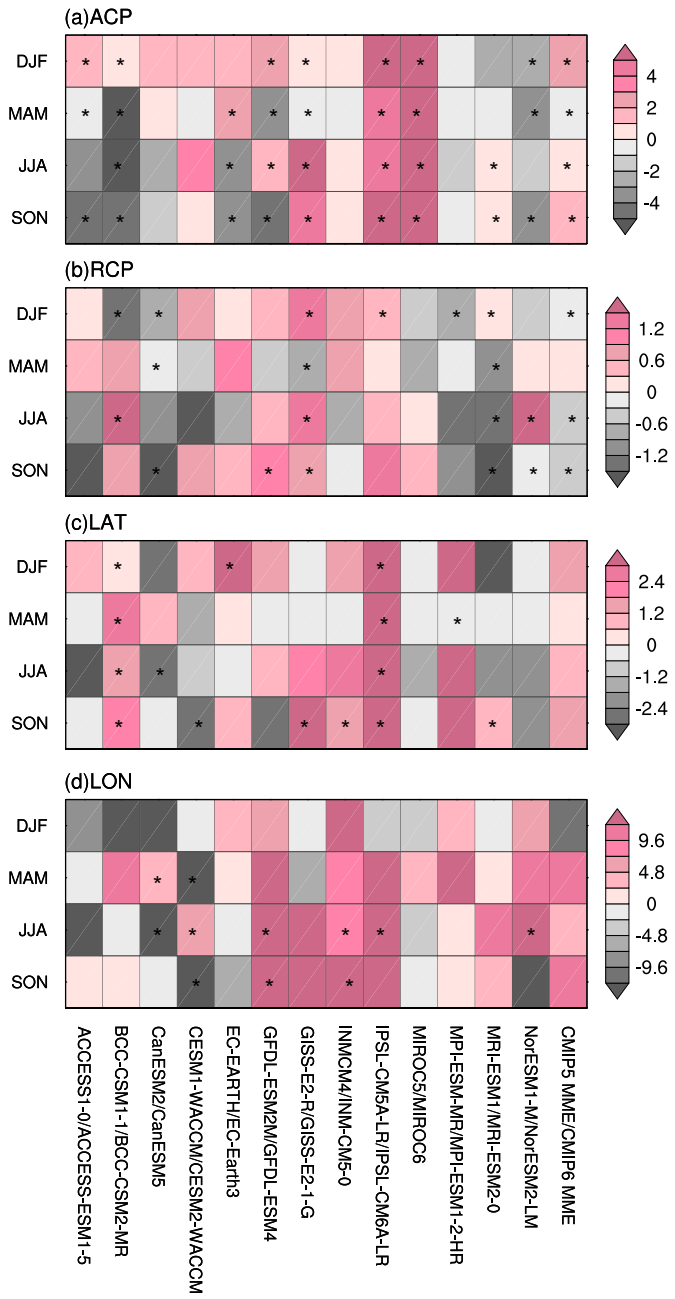

Fig. 5. Differences of the absolute values of seasonal mean biases relative to ERA5 in (a) ACP, (b) RCP, (c) LAT, and (d) LON between CMIP5 and CMIP6 models and MME (CMIP5 minus CMIP6) during 1979–2005, respectively. The stars denote the differences significant at 95% confidence level.

reaches its most southerly position at 77°S in winter (Fig. 4c). Meanwhile, ASL appears over the Bellingshausen Sea with center at 94.25°W in austral summer and shifts westward to the Ross Sea with center persisting around 146.25°W-141.75°W during autumn to the following spring. CMIP MME exhibits reasonable representation of the seasonal evolution of ASL location, although the ASL center shifts 4 degree to the north of that in observation.

As illustrated in Fig. 4, the main features of the ASL annual cycle simulated by both CMIP5 and CMIP6 MME are consistent with observation, except for the relative depth and latitudinal location of ASL center in austral winter. Compared to CMIP5, the ACP, LAT, and LON are better represented in CMIP6 MME. Furthermore, the dispersion of ACP, LAT, and LON simulated by CMIP6 models are much smaller than their CMIP5 versions, which indicates the decreasing uncertainties of ASL simulation in CMIP6 models. Although obvious underestimated RCP and northward shift of ASL could be noticed in JJA, the most significant improvement of simulated uncertainty shown as the band between the maximum and minimum of each ASL index appear in this season.

It is natural to ask which models participating the CMIP6 are improved in depicting ASL from their CMIP5 versions. In order to quantify the improvement, the absolute values of differences between four ASL indices in each model and observation were first calculated, then the biases in CMIP5 models were subtracted from that in their CMIP6 versions. Thus, the positive values indicate that the certain CMIP6 model has better skill in ASL representation than its CMIP5 version, and vice versa. In contrast to CMIP5, the simulation skills of CMIP6 MME in reproducing absolute depth and location of ASL center increase and some models exhibit significant improvements in simulating ASL characteristics during some seasons (Fig. 5). However, individual models' performances differ from each other. More concretely, five CMIP6 models including EC-Earth3, GFDL-ESM4, GISS-E2–1-G, INM-CM5–0 and IPSL-CM6A-LR have made great improvement compared with their CMIP5 versions. They have better performance in capturing ASL features during more than two seasons, though some models even exhibit lower simulation skills.

Different from RCP/LAT/LON, the absolute depth of ASL center exhibits a notable semiannual cycle, with the lowest pressures in April/October and two peaks in January/June, which is consistent with previous studies (e.g., Turner et al., 2013) (Fig. 6). Therefore, whether CMIP models could reproduce this unique feature were further investigated based on monthly ACP. The results show that the semiannual cycle is well reproduced by CMIP models, although the pressure in April is overestimated and the peak of ACP between April and October in CMIP MME and most of individual models delay for one month compared to observation where the peak appears in July. Among all the CMIP6 models, IPSL-CM6A-LR, INM-CM5–0, MRI-ESM2–0, GISS-E2–1-G and MIROC6 make apparent progresses in reducing the relative biases against observation over their CMIP5 versions. The great improvement of these models might also contribute to the raising skills of CMIP6 MME. The current inaccuracy of CMIP6 models is the systematic overestimation/underestimation shown in BCC-CSM2-MR, IPSL-CM6A-LR, CESM2-WACCM, NorESM2-LM, INM-CM5–0, GFDL-ESM4 and MPI-ESM1–2-HR and biases in pressure peaks and valleys shown by ACCESS-ESM1–5, CanESM5, EC-Earth3, GISS-E2–1-G, INM-CM5–0, MIROC6, MRI-ESM2–0 and FGOALS-f3-L.

4. Future projection of ASL under 1.5 °C-4°Cwarming levels based on CMIP6 models

Both the simulated spatial distribution and annual cycle indicate that ASL representation is improved in CMIP6 MME compared to their previous versions and CMIP6 models have a reasonable historical fidelity in capturing climatological features of ASL. Using the improved CMIP6 results, we examined how the ASL features will respond to the global warming. The intensity and location of ASL in the future were investigated based on the ScenarioMIP experiments. The most remarkable feature is the deepening of absolute intensity of ASL in all seasons with degree of global warming (Fig. 7a). The most significant deepening of ASL will occur in austral autumn by around 0.84 hPa, 1.28 hPa, 2.06 hPa and 3.09 hPa from 1.5 °C–4 °C global warming above preindustrial level. Under 3 °C and 4 °C warming worlds, the changes of ACP in all the seasons are significant, which will become 1.08 hPa/2.06 hPa/1.46 hPa/1.08 hPa and 1.47 hPa/3.09 hPa/2.09 hPa/1.63 hPa deeper in DJF/MAM/JJA/SON than the 1995–2014 baseline, respectively. By removing the signal of ASL from atmospheric variability in the background, similar features could be identified in the RCP (Fig. 7b). However, the deepening of ASL relative intensity is only prominent in austral autumn and winter. The relative pressure drops by 0.27 hPa/0.48 hPa/

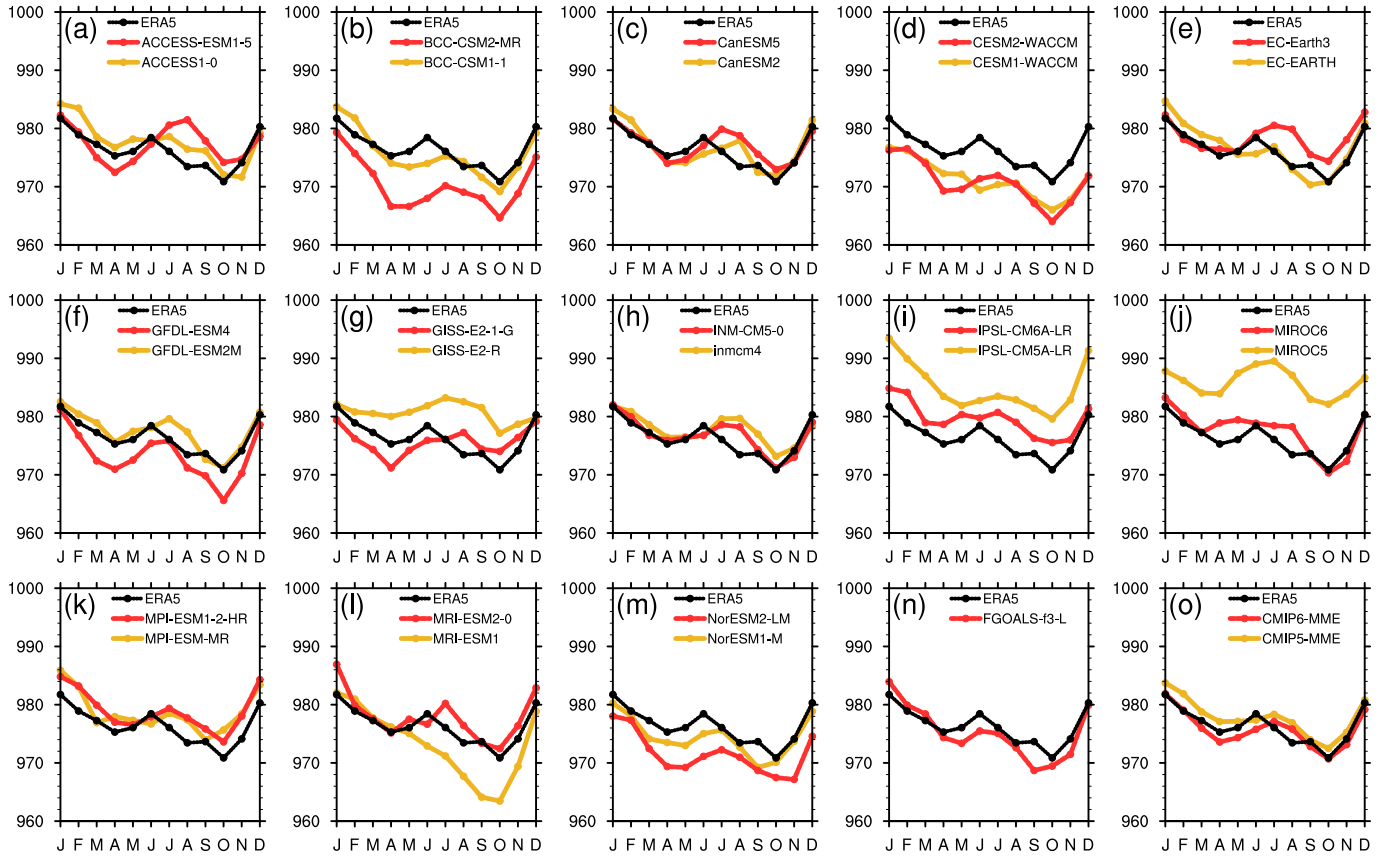

Fig. 6. The ACP derived from ERA5 reanalysis (black), (a) ACCESS1.0/ACCESS-ESM1–5, (b) BCC-CSM1–1/BCC-CMS2-MR, (c) CanESM2/CanESM5, (d) CESM1-WACCM/CESM2-WACCM, (e) EC-Earth/ EC-Earth3, (f) GFDL-ESM2M/GFDL-ESM4, (g) GISS-E2-R/GISS-E2–1-G, (h) INMCM4.0/INM-CM5–0, (i) IPSL-CM5A-LR/ IPSL-CM6A-LR, (j) MIROC5 and MIROC6, (k) MPI-ESM-MR/MPI-ESM1–2-HR, (l) MRI-ESM1/MRI-ESM2–0, (m) NorESM1-M/NorESM2-LM, (n) FOGALS-f3-L, and (o) CMIP5 MME/ CMIP6 MME from January to December during 1979–2005, respectively. The results obtained from CMIP5 models and their CMIP6 versions are shown as yellow and red lines.

0.58 hPa in MAM when the global warming reaches 2 °C/3 °C/4 °C and by 0.39 hPa/0.54 hPa in JJA for 3 °C/4 °C warming thresholds, respectively.

The ASL is simulated to be shifted poleward during austral summer and autumn under high-level warming scenarios (Fig. 7c). Compared to the baseline, the ASL will move southward by 0.67° in DJF under 3 °C global warming and 0.58°, 0.81° and 1.41° in MAM under 2 °C, 3 °C and 4 °C future warming worlds, respectively. Longitudinally westward shift of ASL around 2.94° in MAM under 4 °C warming scenario is expected, but no significant changes in ASL meridional displacement are projected during other seasons (Fig. 7d).

Sea ice plays an important role in the Earth's climate system through ocean-atmosphere heat, mass, and momentum transportation (e.g., Shu et al., 2020). The increasing sea ice trend over the Ross Sea in the sea ice advance season (March–August) during recent decades has attracted extensive attention, because it is counterintuitive to the increase in greenhouse gases. Previous studies have ascribed the sea ice increase over the Ross Sea to the influences of ASL via controlling the meridional wind field (Turner et al., 2009; Hosking et al., 2013; Raphael and Landrum, 2019). Therefore, the ASL indices in sea ice advance season under different warming levels were further examined. The projection shown in Fig. 8 indicates that both of the absolute and relative depth of ASL will deepen in the future. The intensity of ACP will increase from 0.66 hPa, 0.99 hPa, 1.86 hPa to 2.69 hPa with global mean temperature rising from 1.5 °C to 4 °C, and the RCP will enhance significantly from 0.28 hPa, 0.5 hPa to 0.67 hPa under 2 °C to 4 °C warming levels, respectively. The evident poleward shifts of ASL center around 0.42° and 0.66° relative to the baseline are obtained under 2 °C and 4 °C global warming, while the longitudinal change represented by LON is not significant with a large uncertainty during sea ice advance season.

5. Discussion and summary

5.1. Discussion

5.1.1. The possible reasons for the improvement of ASL in CMIP6 models

According to evaluation in Section 3, the simulation skills in ASL mean state of CMIP6 MME have been improved compared to CMIP5. Baines and Fraedrich (1988) found that the formation of ASL could be ascribed to the interaction of the mean westerly flow with the high orography of Victoria Land via a rotating tank experiment. Therefore, to understand why the improvement happens, the Southern Hemisphere westerlies were examined in simulation based on 850 hPa zonal winds from two aspects (Bracegirdle et al., 2017). Fig. 9a and b show the biases of mean westerly flow simulated by CMIP models. Compared to the observation, the simulated westerlies in both of CMIP5 and CMIP6 MME shift equatorward because the zonal winds are significantly underestimated in the areas between 50°S and 70°S but overestimated in the regions around 40°S-50°S, which might relate to the northward displacement of ASL centers in CMIP MME found in Fig. 4c. As a result, the intensity of westerlies in the most of ASL sector were underestimated, which might be responsible for the biases of the ASL depth in CMIP MME shown as Fig. 4a and b. Furthermore, Fig. 9c indicates that the biases of seasonal mean westerly flow simulated by CMIP6 MME against ERA5 are smaller than in CMIP5 MME. This improvement is particularly notable in the ASL sector, suggesting that the skill in

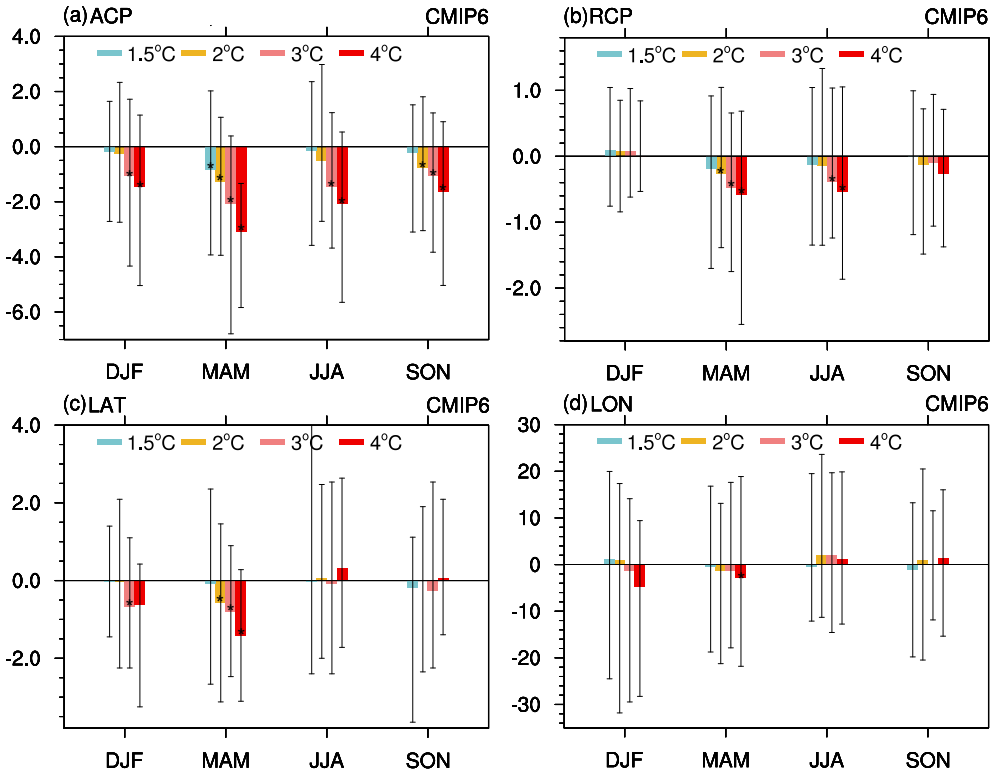

Fig. 7. Projected changes of ASL indices including (a) ACP, (b) RCP, (c) LAT, and (d) LON during DJF, MAM, JJA, and SON in different warming levels relative to the reference period, respectively. Negative values in (c) and (d) indicate southward and westward shifts of ASL, while positive values indicate northward and eastward shifts, respectively. The black lines show the band of values in each ensemble. The color bars with black stars denote the changes of CMIP6 MME are significant at 95% confidence level and more than 70% of ensemble members agree on the sign of MME.

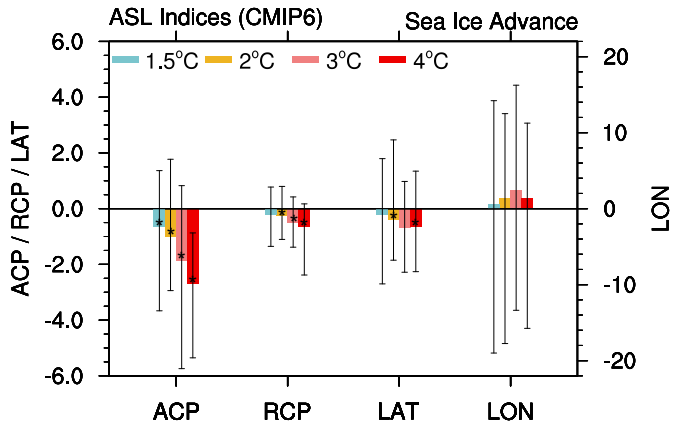

Fig. 8. Projected ASL indices including ACP, RCP and LAT with values in the left y axis and LON with values in the right y axis during sea ice advance seasons (March to August) in different warming levels relative to the reference period. Negative values of LAT indicate southward shifts of ASL, and positive values of LON indicate eastward shifts. The black lines show the band of values in each ensemble. The color bars with stars denote the changes of CMIP6 MME are significant at 95% confidence level and more than 70% of ensemble members agree on the sign of MME.

capturing westerlies might play a fundamental role in generating the ASL in models. The better skills in reproducing the westerlies over ASL sector of EC-Earth3 than MIROC6, which are the best and relative poor performance in representing ASL in CMIP6 models according to Fig. 3, further proves the important contribution of simulated westerlies (Fig. 9d). Meanwhile, compared to other seasons, the largest improvement of CMIP6 MME in simulating westerlies appears in MAM, which is consistent with the models' most prominent increasing skills in reproducing the spatial distribution of ASL in the same season (Fig. 2b). Since many modelling centers participating CMIP6 developed the dynamic core and used the new generation of models (e.g., Krasting et al., 2018; Boucher et al., 2020), the underlying causes remains still unclear and are worth investigating further.

Fig. 4a and b show that CMIP6 models tend to have better skills in capturing the absolute depth of ASL than relative depth. Theoretically speaking, the absolute depth of ASL differs from relative depth because it incorporates the influence of largescale atmospheric mode such as SAM and ENSO while the relative depth doesn't. For instance, since SAM as the dominant mode around Antarctica describes the north-south pressure gradient (Thompson and Wallace, 2000), it could strongly modulate the absolute pressure over ASL region. During ENSO events, ENSO-induced Rossby wave train in the mid-to-high southern latitudes, which is known as the Pacific-South American pattern, places positive or negative geopotential height anomalies over ASL sector (Fogt et al., 2011; Irving and Simmonds, 2016). Through examining the correlation coefficients between monthly ASL central pressure and SAM/ENSO from 1990 to 2000, Hosking et al. (2013) proved that the ACP is significantly related with these broad-scale variabilities, while the correlation coefficients are insignificant between SAM/ENSO and RCP, indicating the influence of atmospheric large-scale variabilities lessened in the RCP after the averaged background pressure is removed. The better representation of the ACP seasonal cycle than that of RCP found in CMIP6 MME further confirms that the impact factors on the absolute and relative depth of ASL might be different (Fig. 4). Why the CMIP6 MME improves simulation skills and reduces uncertainties of ACP but not RCP and whether this is related to the performance of simulated ENSO in CMIP6 models or not deserves further investigation. The reason for the notable bias of latitude of ASL center in austral winter relative to other seasons displayed in Fig. 4c is also worthwhile to be examined in the future.

5.1.2. *The possible impact of future ASL change*

The projections of future ASL based CMIP6 models in Section 4 indicates that ASL will deepen and shift southwestward in some seasons. According to the composite analysis of local atmospheric circulation,

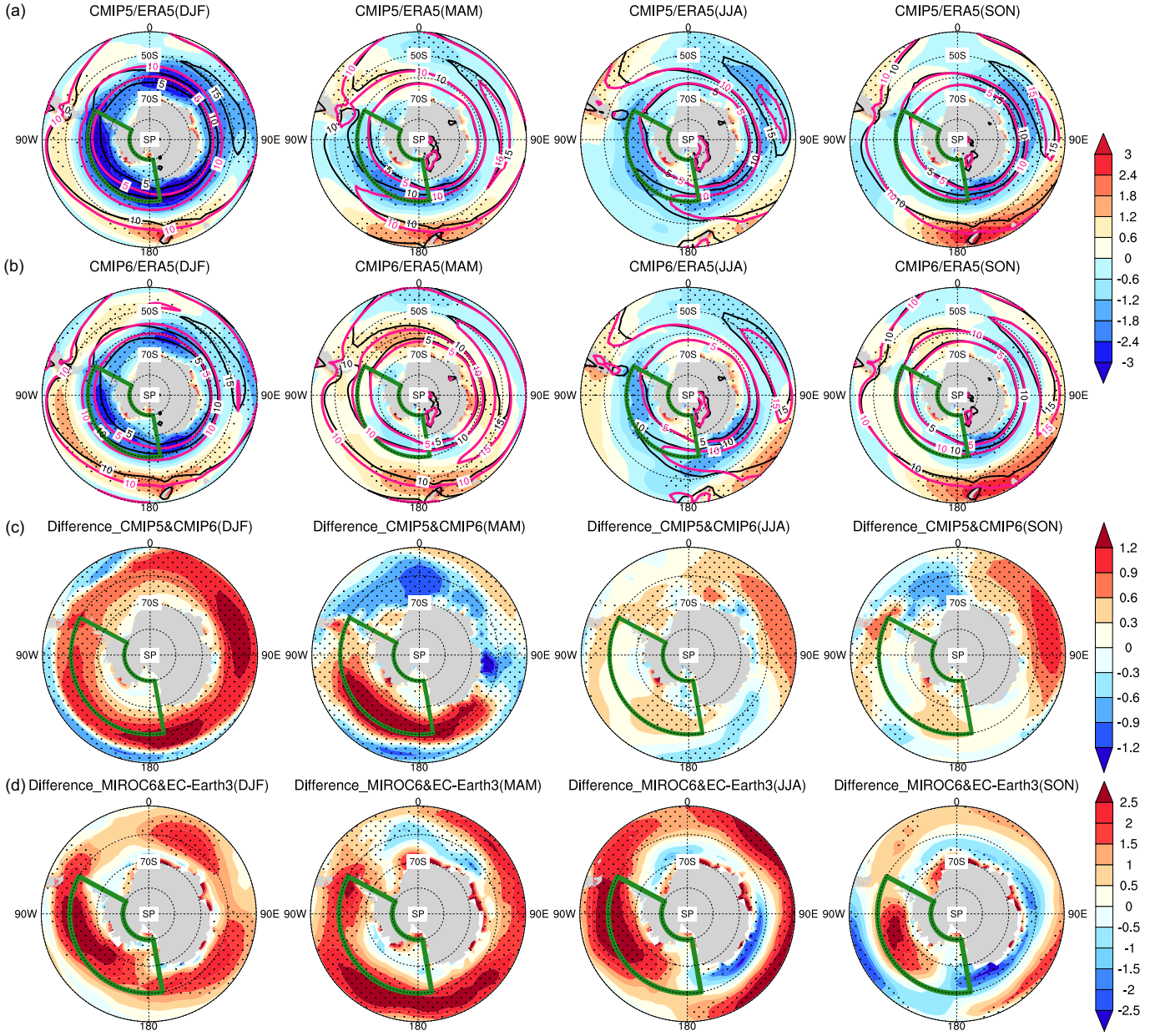

Fig. 9. The seasonal mean biases (relative to ERA5) of 850 hPa zonal winds (shadings: m/s) in (a) CMIP5 MME and (b) CMIP6 MME during DJF, MAM, JJA and SON from 1979 to 2005. The differences of biases in 850 hPa zonal winds (shadings: m/s) between (c) CMIP5 and CMIP6 MME (the absolute values of biases in CMIP5 MME minus that of CMIP6) and (d) MIROC6 and EC-Earth3 (the absolute values of biases in MIROC6 minus that of EC-Earth3) in DJF, MAM, JJA and SON during 1979–2005. Black and pink lines are seasonal mean 850 hPa zonal winds contours by 5 m/s, 10 m/s and 15 m/s that roughly represent location of westerlies in ERA5 and CMIP MME, respectively. The black dots denote the results significant at 95% confidence level. Green rectangles show the ASL sectors.

surface air temperature, and precipitation based on ASL indices (Hosking et al., 2013), the westward movement of ASL strengthens the northerly winds over the Amundsen Sea-eastern Ross Sea, by which warmer and moister conditions extend from ocean to inland due to the advection of warm maritime air. Therefore, we assume that the westward migration of austral autumn ASL might lead to the onshore winds and enhance the warming over the Amundsen Sea-eastern Ross Sea including Ross Ice Shelf in the 4 °C world. Meanwhile, the deepening of RCP in austral winter might lead to a strengthening of northerly flow, which further induce more precipitation over the coastal margins of West Antarctica under high-level global warming scenarios. These results indicate that stronger onshore and northerly winds will provide more heat and moisture to inland west Antarctica in the future. The contrast impact of ASL-associated heat and moisture on the ice sheet mass balance might make the meltwater and ice discharge of West Antarctic Ice Sheet under future global warming more complicated.

Based on the ninth figure in the study of Raphael et al. (2019), during Ross sea ice advance season, the deepening ASL associated with ACP might contribute to the northward expansion of sea ice dynamically via the south/southwesterly flow and result in the increasing sea ice concentration in the center Ross-Amundsen sea sector. By contrast, the RCP-related deeper ASL will lead to less sea ice at the ice edge in the northern and western Ross Sea during this season because it will melt when it is pushed towards the warmer north by southerlies. The role of ACP and RCP changes on the Ross Sea ice is complicated and needs further investigation.

5.2. Summary

By using ERA5 reanalysis dataset and output of newly released CMIP6 models, this study first comprehensively evaluated the climatological characteristics of ASL against observation and compared the models' performance to their CMIP5 versions. In observation, ASL is the deepest of three mean sea level pressure centers around Antarctica comprising the Ross Sea, Amundsen Sea, and Bellingshausen Sea. The spatial distribution of ASL is captured reasonably, but with underestimated relative depth from CMIP6 MME. Among individual CMIP6 models, EC-Earth3 shows the best representation of ASL in four seasons according to both of the pattern correlations and the biases against observation. Four indices, depicting the depth and location of ASL center, including ACP, RCP, LAT, and LON, were further examined to quantify the seasonal evolutions of ASL. The observed ACP reaches its highest/lowest pressure in austral summer/the following spring, while the RCP reaches minimum/maximum in austral winter/summer. In particular, the ACP shows a well-defined semiannual cycle with two deepest valleys in April and October in observation. The seasonal variations of both the absolute and relative depth are well reproduced by CMIP6 MME, although there seems to be systematic biases of RCP in all seasons. CMIP6 MME also captures the seasonal variation of ASL meridional location with northernmost/southernmost points in austral summer/winter and zonal location with an abrupt westward shift in austral summer, except for the 4 degree bias in latitude of ASL center in austral winter. Compared with CMIP5, CMIP6 MME makes improvements in the climatological features of ASL center including absolute depth and location, but not the relative depth. About half CMIP6 models improve the simulation skills, especially the EC-Earth3, GFDL-ESM4, GISS-E2–1-G, INM-CM5–0 and IPSL-CM6A-LR, which results in a better performance of CMIP6 MME and reduced uncertainties.

Based on the new future scenarios proposed in CMIP6, this study further found that the absolute intensity of ASL will very likely deepen with increasing amplitudes of global warming from 1.5 °C to 4 °C in all seasons, while the relative depth might only enhance under high-level global warming conditions in autumn spring. The ASL will also shift southward constantly in austral summer and autumn, when global warming becomes more serious. The significant westward migration of ASL occurs only during austral autumn in 4 °C world. Among all the seasons, the deepening and southwestward shift of ASL will most probably occur in austral autumn. During the Ross sea ice advance season, both of the absolute and relative ASL depths will deepen with increasing intensity and shift poleward under 1.5 °C–4 °C warming levels.

In conclusion, the CMIP6 models reproduce the ASL features reasonably well in comparison to observation and better than CMIP models. In the future, the ASL is expected to deepen and migrate poleward that might influence the atmospheric circulation around west Antarctica and the surrounding ocean, possibly accelerating ice sheet and sea ice melting during some seasons. This study mainly focused on the climatological features of ASL. Since the significant impact of ASL variabilities on climate over West Antarctica has also been found in previous studies, the historical fidelity and future change of variabilities requires further analysis.

Credit author statement

Miaoni Gao: Conceptualization, Formal analysis, Investigation, Writing - Original Draft, Funding acquisition

Seong-Joong Kim: Project administration, Writing - Review & Editing

Jing Yang: Conceptualization, Supervision, Writing - Review & Editing

Jiping Liu: Conceptualization, Writing - Review & Editing

Tong Jiang: Resources, Conceptualization.

Buda Su: Conceptualization

Yanjun Wang: Conceptualization

Jinlong Huang: Methodology

Declaration of Competing Interest

None.

Acknowledgments

This study was supported by the Project PE21030 of Korea Polar Research Institute, the National Natural Science Foundation of China (Grant No. 42022034, 91837101), the Startup Foundation for Introducing Talent of NUIST, the National Key R&D Program of China (Grant No. 2018YFA0605901), and the National Natural Science Foundation of China (Grant No. 41830536). We acknowledge the High Performance Computing Center of Nanjing University of Information Science & Technology for their support of this work. The authors also would like to thank Ms. Shan Xu for her preliminary analysis.

Appendix A. Supplementary data

Supplementary data to this article can be found online at https://doi.org/10.1016/j.atmosres.2021.105533.

References

Baines, P.G., Fraedrich, K., 1988. Topographic effects on the mean tropospheric flow patterns around Antarctica. J. Atmos. Sci. 46, 3401–3415. https://doi.org/10.1175/1520-0469(1989)046<3401:TEOTMT>2.0.CO;2.

Boucher, O., Servonnat, J., Albright, A.L., Aumont, O., Balkanski, Y., Bastrikov, V., Bekki, S., Bonnet, R., Bony, S., Bopp, L., Braconnot, P., Brockmann, P., Cadule, P., Caubel, A., Cheruy, F., Codron, F., Cozic, A., Cugnet, D., D'Andrea, F., Davini, P., de Lavergne, C., Denvil, S., Deshayes, J., Devilliers, M., Ducharne, A., Dufresne, J.-L., Dupont, E., Éthé, C., Fairhead, L., Falletti, L., Flavoni, S., Foujols, M.-A., Gardoll, S., Gastineau, G., Ghattas, J., Grandpeix, J.-Y., Guenet, B., Guez, E., Guilyardi, E., Guimberteau, M., Hauglustaine, D., Hourdin, F., Idelkadi, A., Joussaume, S., Kageyama, M., Khodri, M., Krinner, G., Lebas, N., Levavasseur, G., Lévy, C., Li, L., Lott, F., Lurton, T., Luyssaert, S., Madec, G., Madeleine, J.-B., Maignan, F., Marchand, M., Marti, O., Mellul, L., Meurdesoif, Y., Mignot, J., Musat, I., Ottlé, C., Peylin, P., Planton, Y., Polcher, J., Rio, C., Rochetin, N., Rousset, C., Sepulchre, P., Sima, A., Swingedouw, D., Thiéblemont, R., Traore, A.K., Vancoppenolle, M., Vial, J., Vialard, J., Viovy, N., Vuichard, N., 2020. Presentation and Evaluation of the IPSL-CM6A-LR climate. Model. J. Adv. Model. Earth Syst. 12 https://doi.org/10.1029/2019MS002010 e2019MS002010.

Bracegirdle, T.J., Hyder, P., Holmes, C.R., 2017. CMIP5 diversity in Southern westerly jet projections related to historical sea ice area: strong link to strengthening and weak link to shift. J. Clim. 31, 195–211. https://doi.org/10.1175/JCLI-D-17-0320.1.

Bronselaer, B., Winton, M., Griffies, S.M., Hurlin, W.J., Rodgers, K.B., Sergienko, O.V., Stouffer, R.J., Russell, J.L., 2018. Change in future climate due to Antarctic meltwater. Nature 564, 53–58. https://doi.org/10.1038/s41586-018-0712-z.

Chen, L., Yu, Y., Sun, D.-Z., 2013. Cloud and water vapor feedbacks to the El Niño warming: are they still biased in CMIP5 models? J. Clim. 26, 4947–4961. https://doi.org/10.1175/JCLI-D-12-00575.1.

Dosio, A., Fischer, E.M., 2018. Will half a degree make a difference? robust projections of indices of mean and extreme climate in Europe under 1.5°C, 2°C, and 3°C global warming. Geophys. Res. Lett. 45, 935–944. https://doi.org/10.1002/2017GL076222.

Eyring, V., Bony, S., Meehl, G.A., Senior, C.A., Stevens, B., Stouffer, R.J., Taylor, K.E., 2016. Overview of the coupled model intercomparison project phase 6 (CMIP6) experimental design and organization. Geosci. Model Dev. 9, 1937–1958. https://doi.org/10.5194/gmd-9-1937-2016.

Fogt, R.L., Bromwich, D.H., Hines, K.M., 2011. Understanding the SAM influence on the South Pacific ENSO teleconnection. Clim. Dyn. 36, 1555–1576. https://doi.org/10.1007/s00382-010-0905-0.

Gao, M., Yang, J., Gong, D., He, H., Kim, S.-J., 2016. Spring arctic oscillation-western North Pacific connection in CMIP5 models. Int. J. Climatol. 36, 2093–2102. https://doi.org/10.1002/joc.4486.

Garbe, J., Albrecht, T., Levermann, A., Donges, J.F., Winkelmann, R., 2020. The hysteresis of the Antarctic Ice Sheet. Nature 585, 538–544. https://doi.org/10.1038/s41586-020-2727-5.

Hersbach, H., Bell, B., Berrisford, P., Hirahara, S., Horányi, A., Muñoz-Sabater, J., Nicolas, J., Peubey, C., Radu, R., Schepers, D., Simmons, A., Soci, C., Abdalla, S., Abellan, X., Balsamo, G., Bechtold, P., Biavati, G., Bidlot, J., Bonavita, M., De Chiara, G., Dahlgren, P., Dee, D., Diamantakis, M., Dragani, R., Flemming, J., Forbes, R., Fuentes, M., Geer, A., Haimberger, L., Healy, S., Hogan, R.J., Hólm, E., Janisková, M., Keeley, S., Laloyaux, P., Lopez, P., Lupu, C., Radnoti, G., de Rosnay, P., Rozum, I., Vamborg, F., Villaume, S., Thépaut, J.-N., 2020. The ERA5 global reanalysis. Q. J. R. Meteorol. Soc. https://doi.org/10.1002/qj.3803.

Hosking, J.S., Orr, A., Marshall, G.J., Turner, J., Phillips, T., 2013. The Influence of the Amundsen–Bellingshausen seas low on the climate of West Antarctica and its representation in coupled climate model simulations. J. Clim. 26, 6633–6648. https://doi.org/10.1175/JCLI-D-12-00813.1.

Hosking, J.S., Orr, A., Bracegirdle, T.J., Turner, J., 2016. Future circulation changes off West Antarctica: sensitivity of the Amundsen Sea Low to projected anthropogenic forcing. Geophys. Res. Lett. 43, 367–376. https://doi.org/10.1002/2015GL067143.

IPCC, 2018. Summary for policymakers. In: Global Warming of 1.5°C. An IPCC Special Report on the impacts of global warming of 1.5°C above pre-industrial levels and related global greenhouse gas emission pathways, in the context of strengthening the global response to the threat of climate change, sustainable development, and efforts to eradicate poverty. [Masson-Delmotte, V., P. Zhai, H.-O. Pörtner, D. Roberts, J. Skea, P.R. Shukla, A. Pirani, W. Moufouma-Okia, C. Péan, R. Pidcock, S. Connors, J. B.R. Matthews, Y. Chen, X. Zhou, M.I. Gomis, E. Lonnoy, T. Maycock, M. Tignor, and T. Waterfield (In Press).

Irving, D., Simmonds, I., 2016. A new method for identifying the Pacific–South American pattern and its influence on regional climate variability. J. Clim. 29, 6109–6125. https://doi.org/10.1175/JCLI-D-15-0843.1.

Jiang, Z., Li, W., Xu, J., Li, L., 2015. Extreme precipitation indices over China in CMIP5 models, Part I: model evaluation. J. Clim. 28, 8603–8619. https://doi.org/10.1175/JCLI-D-15-0099.1.

Jun, S.-Y., Kim, J.-H., Choi, J., Kim, S.-J., Kim, B.-M., An, S.-I., 2020. The internal origin of the west-east asymmetry of Antarctic climate change. Sci. Adv. 6 https://doi.org/10.1126/sciadv.aaz1490 eaaz1490.

King, A.D., Harrington, L.J., 2018. The inequality of climate change from 1.5 to 2°C of global warming. Geophys. Res. Lett. 45, 5030–5033. https://doi.org/10.1029/2018GL078430.

Krasting, J.P., John, J.G., Blanton, C., McHugh, C., Nikonov, S., Radhakrishnan, A., Rand, K., Zadeh, N.T., Balaji, V., Durachta, J., Dupuis, C., Menzel, R., Robinson, T., Underwood, S., Vahlenkamp, H., Dunne, K.A., Gauthier, P.P.G., Ginoux, P., Griffies, S.M., Hallberg, R., Harrison, M., Hurlin, W., Malyshev, S., Naik, V., Paulot, F., Paynter, D.J., Ploshay, J., Schwarzkopf, D.M., Seman, C.J., Silvers, L., Wyman, B., Zeng, Y., Adcroft, A., Dunne, J.P., Dussin, R., Guo, H., He, J., Held, I.M., Horowitz, L.W., Lin, P., Milly, P.C.D., Shevliakova, E., Stock, C., Winton, M., Xie, Y., Zhao, M., 2018. NOAA-GFDL GFDL-ESM4 model output prepared for CMIP6 CMIP. https://doi.org/10.22033/ESGF/CMIP6.1407.

Lenton, T.M., Rockström, J., Gaffney, O., Rahmstorf, S., Richardson, K., Steffen, W., Schellnhuber, H.J., 2019. Climate tipping points — too risky to bet against. Nature 575, 592–595.

Luo, Z., Yang, J., Gao, M., Chen, D., 2020. Extreme hot days over three global mega-regions: Historical fidelity and future projection. Atmos. Sci. Lett. https://doi.org/10.1002/asl.1003 n/a, e1003.

O'Neill, B.C., Tebaldi, C., van Vuuren, D.P., Eyring, V., Friedlingstein, P., Hurtt, G., Knutti, R., Kriegler, E., Lamarque, J.-F., Lowe, J., Meehl, G.A., Moss, R., Riahi, K., Sanderson, B.M., 2016. The Scenario Model Intercomparison Project (ScenarioMIP) for CMIP6. Geosci. Model Dev. 9, 3461–3482. https://doi.org/10.5194/gmd-9-3461-2016.

Raftery, A.E., Zimmer, A., Frierson, D.M.W., Startz, R., Liu, P., 2017. Less than 2°C warming by 2100 unlikely. Nat. Clim. Chang. 7, 637–641. https://doi.org/10.1038/nclimate3352.

Raphael, Holland, Landrum, Hobbs, 2019. Links between the Amundsen Sea Low and sea ice in the Ross Sea: seasonal and interannual relationships. Clim. Dyn. 52, 2333–2349. https://doi.org/10.1007/s00382-018-4258-4.

Raphael, M.N., Marshall, G.J., Turner, J., Fogt, R.L., Schneider, D., Dixon, D.A., Hosking, J.S., Jones, J.M., Hobbs, W.R., 2016. The Amundsen Sea Low: variability, change, and impact on Antarctic climate. Bull. Am. Meteorol. Soc. 97, 111–121. https://doi.org/10.1175/BAMS-D-14-00018.1.

Roussel, M.-L., Lemonnier, F., Genthon, C., Krinner, G., 2020. Brief communication: evaluating Antarctic precipitation in ERA5 and CMIP6 against CloudSat observations. Cryosph. 14, 2715–2727. https://doi.org/10.5194/tc-14-2715-2020.

Shu, Q., Wang, Q., Song, Z., Qiao, F., Zhao, J., Chu, M., Li, X., 2020. Assessment of Sea Ice Extent in CMIP6 With Comparison to Observations and CMIP5. Geophys. Res. Lett. 47 https://doi.org/10.1029/2020GL087965 e2020GL087965.

Su, B., Huang, J., Fischer, T., Wang, Y., Kundzewicz, Z.W., Zhai, J., Sun, H., Wang, A., Zeng, X., Wang, G., Tao, H., Gemmer, M., Li, X., Jiang, T., 2018. Drought losses in China might double between the 1.5 °C and 2.0 °C warming. Proc. Natl. Acad. Sci. 115 https://doi.org/10.1073/pnas.1802129115, 10600 LP – 10605.

Taylor, K.E., 2001. Summarizing multiple aspects of model performance in a single diagram. J. Geophys. Res. Atmos. 106, 7183–7192. https://doi.org/10.1029/2000JD900719.

The CMIP6 landscape, 2019. Nat. Clim. Chang. 9, 727. https://doi.org/10.1038/s41558-019-0599-1.

Thompson, D.W.J., Wallace, J.M., 2000. Annular modes in the extratropical circulation, Part I: Month-to-month variability. J. Clim. 13, 1000–1016.

Turner, J., Comiso, J.C., Marshall, G.J., Lachlan-Cope, T.A., Bracegirdle, T., Maksym, T., Meredith, M.P., Wang, Z., Orr, A., 2009. Non-annular atmospheric circulation change induced by stratospheric ozone depletion and its role in the recent increase of Antarctic sea ice extent. Geophys. Res. Lett. 36 https://doi.org/10.1029/2009GL037524.

Turner, J., Phillips, T., Hosking, J.S., Marshall, G.J., Orr, A., 2013. The Amundsen Sea low. Int. J. Climatol. 33, 1818–1829. https://doi.org/10.1002/joc.3558.

United Nations Framework Convention on Climate Change, 2015. Adoption of the Paris agreement. In: United Nations Framework Convention on Climate Change, Paris, p. 31.

Wang, B., Jin, C., Liu, J., 2020a. Understanding future change of global monsoons projected by CMIP6 models. J. Clim. 33, 6471–6489. https://doi.org/10.1175/JCLI-D-19-0993.1.

Wang, S., Liu, J., Cheng, X., Kerzenmacher, T., Braesicke, P., 2020b. Is enhanced predictability of the Amundsen Sea Low in subseasonal to seasonal hindcasts linked to stratosphere-troposphere coupling? Geophys. Res. Lett. 47 https://doi.org/10.1029/2020GL089700 e2020GL089700.

Zhang, W., Zhou, T., Zou, L., Zhang, L., Chen, X., 2018. Reduced exposure to extreme precipitation from 0.5 °C less warming in global land monsoon regions. Nat. Commun. 9, 3153. https://doi.org/10.1038/s41467-018-05633-3.